Burst Oscillation Periods from 4U 1636–53: A Constraint on the Binary Doppler Modulation

A. B. Giles[1,2], K. M. Hill[1], T. E. Strohmayer[3], N. Cummings[3]

[1] *School of Mathematics and Physics, University of Tasmania*
GPO Box 252-21, Hobart, Tasmania 7001, Australia
Barry.Giles@utas.edu.au, Kym.Hill@utas.edu.au

[2] *Spurion Technology Pty. Ltd. 200 Mt. Rumney Road, Mt. Rumney, Tasmania 7170, Australia*

[3] *Laboratory for High Energy Astrophysics, Mail Code 662 NASA Goddard Space Flight Center, Greenbelt, MD 20771, USA*
stroh@clarence.gsfc.nasa.gov, nickc@pcasrv1.gsfc.nasa.gov

ABSTRACT

The burst oscillations seen during Type I X-ray bursts from low mass X-ray binaries (LMXB) typically evolve in period towards an asymptotic limit that likely reflects the spin of the underlying neutron star. If the underlying period is stable enough, measurement of it at different orbital phases may allow a detection of the Doppler modulation caused by the motion of the neutron star with respect to the center of mass of the binary system. Testing this hypothesis requires enough X-ray bursts and an accurate optical ephemeris to determine the binary phases at which they occurred. We present here a study of the distribution of asymptotic burst oscillation periods for a sample of 26 bursts from 4U 1636-53 observed with the Rossi X-ray Timing Explorer (RXTE). The burst sample includes both archival and proprietary data and spans more than 4.5 years. We also present new optical light curves of V801 Arae, the optical counterpart of 4U 1636-53, obtained during 1998-2001. We use these optical data to refine the binary period measured by Augusteijn et al. (1998) to 3.7931206(152) hours. We show that a subset of $\sim 70\%$ of the bursts form a tightly clustered distribution of asymptotic periods consistent with a period stability of $\sim 1 \times 10^{-4}$. The tightness of this distribution, made up of bursts spanning more than 4 years in time, suggests that the underlying period is highly stable, with a time to change the period of $\sim 3 \times 10^4$ yr. This is comparable to similar numbers derived for X-ray pulsars. We investigate the period and orbital phase data for our burst sample and show that it is consistent with binary motion of the neutron star with $v_{ns} \sin i < 38$ and 50 km s^{-1} at 90 and 99% confidence, respectively. We use this limit as well as previous radial velocity data to constrain the binary geometry and component masses in 4U 1636-53. Our results suggest that unless the neutron star is significantly more massive than 1.4 $M_\odot$ the secondary is unlikely to have a mass as large as 0.36 $M_\odot$, the mass estimated assuming it is a main sequence star which fills its Roche lobe. We show that a factor of ~ 3 increase in the number of bursts with asymptotic period measurements should allow a detection of the neutron star velocity.

Subject headings: Binaries; general - Stars: individual (4U 1636-53) - Stars; neutron - X-rays; stars

1. Introduction

Millisecond oscillations in the X-ray brightness of thermonuclear X-ray bursts (so called "burst oscillations") have now been reported for 10 low mass X-ray binary (LMXB) systems (see Strohmayer 2001 for a review). All of these results are based on observations with the Proportional Counter Array (PCA) on the Rossi X-ray Timing Explorer (RXTE) except for the evidence for burst oscillations from the accreting millisecond pulsar SAX J1808-369 which is based on SAX Wide Field Camera data (see in't Zand et al. 2001). A large body of evidence supports the hypothesis that these oscillations are produced by rotational modulation of a hot spot (or possibly a pair of hot spots) induced on the neutron star surface by inhomogeneous nuclear burning. In particular, the large modulation amplitudes, high coherence and long term stability of the frequency are fully consistent with the rotational modulation scenario (see Strohmayer, Zhang & Swank 1997; Strohmayer et al. 1998a; Strohmayer & Markwardt 1999; Muno et al. 2000 and Strohmayer et al. 1998b).

The oscillation frequency during a burst is usually not constant. Often the frequency is observed to increase by $\approx 1-3$ Hz in the cooling tail, reaching a plateau or asymptotic limit. Strohmayer et al. (1997) have suggested that the time evolution of the burst oscillation frequency results from angular momentum conservation of the thermonuclear shell. The burst expands the shell, increasing its rotational moment of inertia and slowing its spin rate. Near burst onset the shell is thickest and thus the observed frequency lowest. The shell spins back up as it cools and recouples to the underlying neutron star. Cumming & Bildsten (2000) studied this mechanism in some detail and concluded that it appeared to be viable. However, more recent work by Cumming et al (2001) which corrects an error in their previous work and includes general relativistic effects suggests that it may not be able to account for all of the observed frequency evolution. Spitkovsky, Levin & Ushomirsky (2001), however, suggest that geostrophic effects due to the coriolis force and local thermonuclear heating will generate zonal winds which can also influence the frequency evolution. In fact, they suggest that these effects may be comparable to those caused by radial uplift alone. Heyl (2001) has suggested that r-modes, which are retrograde oscillations, may be responsible for the asymmetry which produces the oscillations in the tails of bursts. Since r-modes are retrograde they will preferentially produce frequency decreases. Although the exact scenario for frequency evolution is still not agreed upon, substantial evidence suggests that the limiting frequency is the neutron star spin frequency. In the context of this paper we will regard this as a good working hypothesis. We note, however, that not all bursts exhibit this spin up behavior. For example, Strohmayer (1999) and Miller (2000) identified a burst from 4U 1636-53 (burst 4 in Table 3) with a spin down of the oscillations in the decaying tail. This burst also had an unusually long decaying tail which may have been related to the spin down episode. Muno et al. (2000) also reported an episode of spin down in a burst from KS 1731-260.

The long term (over year timescales) stability of burst oscillations from 4U 1728-34 and 4U 1636-53 has been studied by Strohmayer et al. (1998b). For three bursts from 4U 1728-34 separated in time by ≈ 1.6 years they found the 363 Hz burst frequency to be highly stable, with an estimated time scale to change the oscillation period of about 23,000 years. Based on a study of three bursts from 4U 1636-53 (bursts number 1, 2 & 3 in Table 3) spanning a much shorter time interval (about 1 day) they suggested that the observed changes in the limiting frequency of the 581 Hz oscillation might be due to orbital motion of the neutron star, which could provide a way of deriving or constraining the X-ray mass function of the system. However, with only three bursts available at the time it was not possible to test this hypothesis definitively nor draw any strong conclusions on the mass function. 4U 1636-53 is perhaps the best system in which to search for such an effect since the orbital period is known and a large sample of bursts have now been obtained with RXTE. For plausible system parameters and the orbital period of $\sim$3.8 hours the expected Doppler shifts are of order a part in 10^{-4}.

The optical counterpart of 4U 1636-53, V801 Arae, has been observed many times since its identification in 1977 (McClintock et al. 1977; Jernigan et al. 1977) and a collection of photometric data, from July 1980 to May 1988, was compiled by van Paradijs et al. (1990) (see references therein). The van Paradijs et al. (1990) ephemeris was later revised by Augusteijn et al. (1998) who identified a cycle miss count by reanalysing all the old data and incorporating newer observations made between June 1992 and August 1993. Augusteijn et al. (1998) also reported some spectroscopic measurements of emission and absorbtion line features.

In this paper we report new photometric light curves of 4U 1636-53 obtained over the period 1998 March to 2001 May and use them to revise the ephemeris of Augusteijn et al. (1998). We then use this new emphemeris to derive the binary phases of RXTE X-ray bursts and examine the possibility that the distribution of observed asymptotic burst oscillation periods is consistent with Doppler modulation caused by the orbital velocity of the neutron star. The paper is organized as follows. In §2 we begin with a discussion of our new optical observations. We then explore in §3 the implications of our new observations for the ephemeris of maximum light from V801 Arae. We show that our data suggest a small correction to the orbital period of Augusteijn et al. (1998). In §4 we describe the sample of X-ray bursts from 4U 1636-53 and we study in detail the observed distribution of asymptotic burst oscillation periods. We show that a subset of $\approx 70\%$ of bursts with asymptotic period measurements form a tightly clustered distribution consistent with having been generated by a highly stable underlying period. We then fit this distribution to models of the period - phase distribution expected from binary motion of the neutron star and show that it is consistent with circular orbital motion of the neutron star with $v \sin i < 38$ km s^{-1} (90% confidence). In §5 we summarize our findings and discuss their implications for the component masses and binary geometry of 4U 1636-53. We conclude with a discussion of future improvements to our constraints expected from a larger sample of X-ray bursts.

2. Optical Observations

All the optical observations described in this paper were made using the Mt. Canopus 1-m telescope at the University of Tasmania observatory. The observations used standard V & I filters and the CCD reduction procedure was identical to that described in Giles, Hill & Greenhill (1999). All times presented in this paper have been corrected to Heliocentric Julian Dates (HJD) and a complete journal of the observations is given in Table 1. For the 1998 observations the telescope was equipped with an SBIG CCD camera having 375 x 242 pixels with an image scale of $0.42'' \times 0.49''$ pixel^{-1}. On the nights of 1998 March 25 & 27 continuous pairs of V & I integrations were obtained but the I band data are not discussed further in this paper. Three V band light curves from 1998 are shown in Figure 1 which plots the differential magnitudes with respect to a brighter star that can be located on the finder chart in Jernigan et al. (1977). This secondary standard is at the western end of the $20''$ scale bar (see Figure 2 on their 2S1636-536 chart). 4U 1636-53 is star number 3 on this same chart and is ~ 1.8 V magnitudes dimmer than our secondary standard. For the 1999 and later observations the telescope was equipped with an SITe CCD camera having 512 x 512 pixels with an image scale of $0.42''$ pixel^{-1}. The reduction procedures for these observations were similar to the 1998 data and the same local secondary standard was used. In Figure 2 we show the light curves for the nights of 1999 June 9 and 2001 May 7 & 8. We do not show plots for the remaining nights listed in Table 1 since the individual time spans are rather limited.

3. Optical Ephemeris

The ephemeris for times of maximum optical light given by Augusteijn et al. (1998) is HJD = 2446667.3183(26) $\pm$ [N $\times$ 0.15804738(42)] where the errors are indicated in the round brackets. This ephemeris was based on observations made between 1980 July 11 and 1993 July 12 and covers a total of 30048 binary periods. The predictions for this ephemeris are shown on Figures 1 & 2 as the dotted traces in the lower sections of each light curve panel. We have fitted a sine curve to each nights' observations listed in Table 1 taking the amplitude, phase and mean as free parameters but fixing the binary period at the value given by Augusteijn et al. (1998). From these sine fits we derive the times of optical maxima listed in Table 2. This table is intended to be complimentary to the similar Table 2 of Augusteijn et al. (1998) and the cycle numbers continue the same sequence. Although we tried to fit sine curves to all the nights listed in Table 1 a few of them have insufficient data and are not included in Table 2. The appropriate sine curve fits are also shown plotted through the respective data points in Figures 1 & 2. There is a small phase shift evident between our new data and the Augesteijn et al. (1998) prediction when extrapolated forward in time for the additional ~18080 binary periods to 2001 May. The times of observed maxima are consistently earlier than expected.

To quantify this change and derive a new ephemeris we show in Figure 3, in the conventional way, the observed minus calculated (O-C) times of optical maxima plotted against time. This plot

combines the data from our Table 2 with that of Table 2 from Augusteijn et al. (1998) and there is considerable scatter in the O-C phase values as they had also noted. Using the Augusteijn et al. (1998) ephemeris for a similar plot to Figure 3 places all our new data below the zero phase line since the observed maxima are clearly arriving too early. We have performed both linear and 2nd order polynomial fits to the combined data but the higher order fit is not warrented due to the large scatter. We adjusted the ephemeris parameters to place the best linear fit through the data points to lie along the zero phase axis as shown in Figure 3. We therefore adopt the following new ephemeris for the times of maximum optical light from 4U 1636-53: HJD = 2446667.3179(33) $\pm$ [N $\times$ 0.15804693(16)]. The small period change in our refined ephemeris is approximately the size of the period error quoted by Augusteijn et al. (1998). The night of 1998 April 3 in Figure 1 does have an odd profile but van Paradijs et al. (1990) have previously commented on multi-humped profiles which they had eliminated from their analysis procedure. Phase zero is particularly hard to define for this system where the light curve is quite variable and has no sharp repeating eclipse type feature. We have therefore decided to adopt a conservative estimate of $\pm$0.04 for the X-ray burst phase errors listed in Table 3 and used in subsequent sections of this paper. We note that despite the absolute phase uncertainties of the X-ray bursts their relative phases are well defined for the purposes of this paper. In any case there is still an unknown relationship between the optical and true orbit phase zero which we comment on further in a later section. Throughout this paper phase zero is defined as the optical maximum when superior conjunction of the companion star is thought to occur (neutron star closest to the Earth). With no significant period derivative we are unable to improve on the P / $\dot{P}$ value of $\geq 3 \times 10^5$ years given by Augusteijn et al. (1998).

4. Asymptotic Oscillation Periods of RXTE X-ray Bursts

A total of 30 X-ray bursts from 4U 1636-53 are available to us as public or PI data from the PCA experiment on RXTE and information about them relevant to this study are listed in Table 3. A comprehensive description of the properties of these bursts will be given elsewhere (Cummings & Strohmayer 2001). Here we will be primarily interested in the asymptotic burst oscillation periods and inferred binary orbital phases of the bursts. The 1.72 ms (581 Hz) oscillation in most of these bursts exhibits a characteristic evolution towards a limiting (shortest) period in the tail of the burst. It was our aim to try and measure this limiting period for each burst in the sample. For most of these bursts we had event mode data with a time resolution of 1/8192 seconds across the entire 2 - 60 keV PCA bandpass. In a few cases we had binned data with the same time resolution. We began by correcting the event arrival times to the solar system barycenter using the JPL DE200 ephemeris and the standard RXTE analysis tools (either fxbary, or faxbary for the most recent data). We then calculated dynamic variability spectra using the Z_1^2 statistic (see Strohmayer & Markwardt 1999 for a discussion and example). Such spectra are essentially similar to standard FFT dynamic power spectra except that we oversample in frequency. We used 2 s intervals and start a new interval every 0.125 s. We oversample in frequency by a factor of 16. For each burst we calculated two dynamic spectra, one using data across the entire bandpass, and a second using only

a hard band from 7 – 20 keV. We did this because burst oscillation amplitudes are often stronger at higher energies (see for example Strohmayer et al. 1997). To determine the asymptotic period we searched the pair of dynamic power spectra of each burst and determined the shortest period detectable during each burst. By detectable we mean that the signal peak had to be larger than $Z_1^2 > 16$, which corresponds to a single trial significance of 3.4×10^{-4}. As an example Figure 4 shows a typical dynamic spectrum from one of our bursts and the power spectrum from which the asymptotic period was deduced (burst 20 in Table 3, in this case the spectrum from the hard band). In most cases a clear frequency track of the oscillation could be seen in the dynamic power spectrum, and the procedure was relatively straightforward. In several cases, either the oscillations were very weak or the frequency evolution was "anomalous" (meaning the frequency was observed to decrease with time), and in these cases we judged that an asymptotic period could not be reliably measured. An example of this is the burst which occurred on 1996 December 31 (burst 4 in Table 3) and has been discussed in detail by Strohmayer (1999). We note that this was the case for only 4 bursts in our sample, so that in the majority of cases the asymptotic period was reasonably well defined. Although these bursts could not be used for the present investigation, for completeness, we also include them in Table 3. We selected the shortest asymptotic period measured in either power spectra as the asymptotic value for that burst. These periods are also listed in Table 3.

The column in Table 3 showing the burst binary phases has been derived using the new optical ephemeris described in the previous section. The phase error for each burst is dominated by the ability to determine the optical phase zero for any particular epoch but is typically $< \pm 0.04$. Relative phase errors amongst the data are much smaller given the >48,000 cycle time span of the optical observations and the fact that the X-ray bursts used here all occur within a time interval of ~ 4.4 years (only 10,000 cycles) ending in 2001 May.

4.1. Period Measurement Uncertainty

An important quantity to understand is the characteristic error, σ_P, in our period measurements. To estimate this we have carried out a series of simulations which mimic the conditions of our asymptotic period measurements. To do this we first generate a count rate model comprised of a constant plus a sinusoidal modulation of fixed period and amplitude. We then generate random realizations of this model using the same temporal resolution as our burst data. We model a 2 s interval of data since this was the interval length we used for all our dynamic spectra. We use a count rate and modulation amplitude typical of the intervals in the tails of bursts where we actually measure the asymptotic periods. We then compute the Z_1^2 spectra for each of the simulated data sets and determine the centroid period of the signal. Since typically we follow the signal in a real burst down to or near a limiting threshold (in this case $Z_1^2 = 16$), we only keep simulated period measurements for which the peak signal power was close to our limiting threshold. In practice we found that $16 < Z_1^2 < 24$ was characteristic of our actual asymptotic period measurements. We then determine how these simulated periods are distributed around the true period. Specifically

we fit a gaussian to the distribution of simulated periods and identify the width of this gaussian with the characteristic uncertainty, σ_P, in any one of our period measurements. Figure 5 shows the period distribution and best fitting gaussian derived from one of these simulations. We find that the typical measurement error associated with one of our periods is $\sim 2.2 \times 10^{-4}$ ms. Note that this is purely a statistical uncertainty. Another source of possible systematic error is associated with the assumption that the last period detected in a dynamic spectra represents a limiting value. We will have more to say on this in a later section.

4.2. The Observed Distribution of Asymptotic Periods

We used the period measurements from Table 3 to construct a distribution of asymptotic periods. Figure 6 shows a histogram representation of the distribution. Although the range of all observed periods is rather large, a subset of $\sim 70\%$ of the bursts form a tightly peaked distribution. Also shown in Figure 6 is the gaussian model which best fits this cluster of periods. The gaussian is centered at $1.71929 \pm 1.0 \times 10^{-4}$ ms, has a width of $2.3 \times 10^{-4} \pm 1.2 \times 10^{-4}$ and gives an excellent fit to the data. This subset is comprised of bursts from all epochs of our sample, and suggests that a highly stable underlying period is responsible for this component of the asymptotic period distribution. Note also that the width of this distribution is comparable to our estimate above of the typical width which would be produced by statistical uncertainties alone. This suggests that any systematic error associated with our measurements not reflecting a true limiting value are small, at least within this subset of the entire sample.

4.3. A Constraint on the Orbital Doppler Modulation

Assuming that the burst oscillations do reflect the spin of the neutron star the binary motion should imprint doppler modulations on the measured periods. We use the values from Table 3 to construct in Figure 7 a plot of asymptotic period against photometric phase. Phase zero in the plot corresponds to optical maximum. Visual inspection of this plot reveals no obvious sinusoidal component that might be produced by a sufficiently strong Doppler modulation. Assuming that photometric maximum occurs at superior conjunction of the secondary, such a modulation would have a peak on Figure 7 at a phase of 0.25. We tested this conclusion quantitatively by fitting a period - phase model to the data. We used the model

$$P_i = P_0 \left(1 + (v \sin i/c) \cos(2\pi(\phi_i - \phi_{dyn}))\right), \qquad (1)$$

where P_i, P_0, $v \sin i$, ϕ_i, and ϕ_{dyn} are the asymptotic period measured for burst i, the period measured at inferior conjunction of the neutron star (neutron star nearest to observer), the projected orbital velocity of the neutron star with respect to the center of mass of the binary, the orbital phase at which burst i occurred, and the phase of maximum recessional velocity of the neutron star, respectively. Figure 7 shows the results of our fits. With ϕ_{dyn} fixed at 0.25 (this assumes

that maximum optical light occurs at superior conjunction of the secondary) the model prefers a small $v \sin i/c = 5.5 \times 10^{-5}$ (16.5 km s^{-1}), with $\chi^2 = 20.3$ for 16 degrees of freedom. This model is the solid curve in Figure 7. The probability that such a value could arise by chance is $\sim 21\%$, so the model gives an acceptable description of the data. A fit with $v \sin i/c \equiv 0$, however, has $\chi^2 = 21.9$, and with 17 degrees of freedom is only marginally worse than the fit with non-zero velocity (probability of 18.7%). From this we conclude that the data are consistent with no doppler modulation, however, we can place an upper limit on the velocity. The 90% and 99% confidence upper limits ($\Delta\chi^2 = 2.71$ and 6.63) on $v \sin i$ are 38 and 50 km s^{-1}, respectively. The models with $v_{ns} \sin i = 38$ and 50 km s^{-1} are the thick dashed curves in Figure 7. Note that these fits assumed that $\phi_{dyn} \equiv 0.25$, that is, the relative phase of the modulation is known based on the assumption that optical maximum occurs at superior conjunction of the secondary. If we relax this assumption and allow the phase of the peak modulation to vary we find a better fit with $v \sin i = 35.4 \pm 15$ km s^{-1} (dotted curve in Figure 7), and a reference phase of $\phi_{dyn} = 0.415 \pm 0.06$. This fit has $\chi^2 = 16.12$ and with 15 degrees of freedom has a chance probability of 37.5%. The phase offset is 0.165 away from that implied under the assumption that phase zero (photometric maximum) is at superior conjunction of the secondary. Although this seems large it might be possible if X-ray heating of the disk bulge and accretion stream interaction region contribute to the observed optical modulations. We discuss this further below.

Although we do not detect any doppler modulation we were able to place an upper limit on $v \sin i$ from the period - phase data. Since there was no strong evidence for a modulation with orbital phase we also investigated the upper limit using only the expected distribution of periods for a given $v_{ns} \sin i$ and σ_P. To do this we generated an expected period distribution by sampling a large number of random periods from the model. Samples were drawn uniformly in orbital phase and the random period was selected from a gaussian distribution with width σ_P centered on the model period for that phase. We then binned the sample periods in the same manner as the data and computed a χ^2 goodness of fit statistic $\chi^2 = \sum_j (O_j - M_j)^2/M_j$. Since our data have small numbers of events in each bin we computed the upper limit for $v_{ns} \sin i$ using monte carlo simulations. Our resulting upper limit using this method is in good agreement with our result from the period versus phase fits.

5. Summary and Discussion

We have investigated the asymptotic period distribution of burst oscillations in a large sample of bursts from 4U 1636-53. We find that $\sim 70\%$ of these bursts form a tight distribution consistent with being produced by a highly stable mechanism such as rotation of the neutron star. The fact that the distribution is made up of bursts spanning a time scale of 4.4 years and has a characteristic width of $\Delta P/P = 1.3 \times 10^{-4}$ indicates that the time scale to change the underlying period is $\tau > \Delta T P/\Delta P = 3.4 \times 10^4$ yr. This is comparable to the overall period stability estimated for the 363 Hz oscillations in 4U 1728-34 (see Strohmayer et al. 1998b), and is a number characteristic of

other rotating neutron stars such as X-ray pulsars. This provides further evidence that rotation of the neutron star sets the burst oscillation period.

Why do some of the bursts fall well outside this distribution? It seems likely that several effects may be at work here. One problem is that the oscillation in some bursts does not remain strong enough to detect for a long enough time interval within the burst, so that the asymptotic limit is not reached. This results because burst oscillation properties are not identical from burst to burst. Another possible effect was discussed by Cumming & Bildsten (2000). They argued that as long as the burning shell was not recoupled to the neutron star the frequency observed in the burst tail would deviate slightly (by about 1 part in 10^{-4}) from the neutron star spin frequency. This comes about because the thickness of the cooling atmosphere in the tail is different to the initial thickness by about 1 m, though the exact amount depends on the mean molecular weight of the burned material which in turn depends on how complete the burning was and would be expected to vary from burst to burst. Although this could conceivably be a source of additional scatter in the asymptotic periods the fact that our observed distribution has a width comparable to that expected based on statistical uncertainty alone suggests that if operating at all it must be small. If the asymmetry on the star is created by a nonradial oscillation mode (see for example Bildsten & Cutler 1995; Strohmayer & Lee 1996; Heyl 2001), then the observed oscillation frequency would always be close to the spin frequency or perhaps a multiple $m\Omega$ of it, but it could change by ~ 1 Hz due to long term changes in the surface layers of the neutron star. This could produce outliers in the period distribution, but would also tend to produce a tight component as long as surface conditions were similar for enough bursts. If r-modes are involved as suggested by Heyl (2001), then one would expect, preferentially, that the period distribution would favor periods longward of the spin period and not shortward, as observed. Recently, Spitkovsky, Levin & Ushomirsky (2001) have also studied mechanisms which can cause frequency drift. They suggest that Coriolis forces can have an important effect and might introduce shifts in the observed frequency comparable to those expected from radial uplift.

5.1. Constraints on the Binary Geometry

In general the optical flux from LMXBs is thought to be dominated by the accretion disk (see van Paradijs & McClintock 1995 for a review). There are three regions of a LMXB system which might contribute to its optical variability due to X-ray heating. These are the accretion disk itself, a bright spot or bulge on the outer edge of the accretion disk formed by interaction of the accretion stream with the disk, and the hemisphere of the companion facing the neutron star which is not shadowed by the accretion disk. In LMXBs with relatively low inclinations ($i \lesssim 60°$) it is this last region which is thought to dominate the optical modulations from the rest of the system (van Paradijs 1983, van Paradijs & McClintock 1995). These systems generally produce roughly sinusoidal optical modulations. The optical maximum is thought to occur when the companion is on the far side of the neutron star (superior conjunction) but there may be some asymmetry or

variation about the mean profile due to gas flows causing various X-ray shielding effects (Pedersen et al. 1982a).

In order to explore the implications for the binary geometry of our radial velocity limit for the neutron star we have created in Figure 8 a plot of the Roche geometry for 4U 1636-53. For the neutron star we assumed a mass of $1.6M_{\odot}$. For the secondary we use a mass of $0.36M_{\odot}$ (see Smale & Mukai 1988; Patterson 1984). With these masses and the known 3.8 hr orbital period the binary separation is $\sim 1.58R_{\odot}$. The velocities of the neutron star and secondary with respect to the center of mass would be 91 and 390 km s^{-1}, respectively. Figure 8 shows a view looking down on the orbital plane of the system. The numbers circling the system denote orbital phases assuming phase zero occurs at superior conjunction of the secondary. We note that this may not necessarily correspond to photometric maximum. In this figure the system should be thought of as rotating in the clockwise sense. Alternatively, one can think of the observer advancing around the opposite way in the direction of the increasing phase numbers. With such an orientation, the accretion stream will indeed be directed toward figure bottom (ie. toward the shaded region in the disk, see, for example, Figure 1 of Lubow & Shu 1975). The dashed circle shows the extent of a disk which fills $\sim 90\%$ of the Roche lobe, a radius at which it will likely be truncated due to tidal effects (see for example Frank, King & Lasota 1987). Constraints from analysis of optical reprocessing of X-ray bursts also indicate a large accretion disk in 4U 1636-53 (Pedersen et al. 1982a).

We also show on the plot inferred locations of the radial velocity components measured by Augusteijn et al. (1998) and given in their Table 6. Since the inferred velocity amplitudes from their three sets of fits were all rather similar we just used the average velocity as well as the average uncertainty. We plotted with triangles the $\pm 1\sigma$ average velocity amplitude at the phases of superior conjunction given for each of their three fits. Note that the phase of superior conjunction is the position at which the emitting matter is *furthest* from the observer. We also shaded the region enclosed by the triangles to further highlight its location. In deriving these locations we assumed that the velocities of the emission line components are dominated by their motions with respect to the center of mass of the binary. In effect, this assumes that matter in the binary rotates rigidly about the center of mass. This cannot be strictly correct, since the disk must rotate about the neutron star, however, since the radial velocity components are long lived they must arise from some physical structure which is fixed in the rotating frame on timescales longer than the binary period (as for example, the bulge in the disk). Augusteijn et al. (1998) suggested the radial velocity components could be identified with the bulge region associated with the interaction of the accretion stream with the disk. Our plot certainly supports this suggestion, since the shaded region is consistent with where the accretion stream would likely impact the disk. Moreover, it also suggests, at least indirectly, that our assumptions in deriving the radial velocity locations are not too unreasonable.

The location of the shaded region also suggests that the bulge might be a significant component with regard to optical modulations. Our fits with the phase, ϕ_{dyn}, of maximum neutron star recessional velocity as a free parameter suggest that this occurs 0.41 in phase after photometric

maximum. This would imply that maximum light occurs with the observer close to phase ~ 0.85 in Figure 8, when the X-ray illuminated portion of the bulge is facing the observer. More detailed modelling would be required to determine if the bulge can indeed effect the optical modulations at this level, but the period - phase fits are suggestive. We also note that although the three simultaneous X-ray & optical bursts discussed by Pedersen et al. (1982a) (see page 336) have relatively large error bars on the optical time delays we have re-examined them in the light of our new ephemeris and the system model shown in Figure 8. The optical delays in these bursts appear more consistent, both in delay and phase, with the reprocessed X-ray burst optical flux coming from the outer parts of our shaded region in Figure 8 than from the facing hemisphere of the companion star. Although there is no evidence of a second optical pulse from the companion in the many optical bursts studied by Pedersen et al. (1982b) a weaker following pulse might easily be lost. Such a pulse might only be evident at optimum binary phases, around phase 0.85, with reprocessing delays always tending to broaden and confuse the pulse light curve features.

Although the radial velocities of the neutron star and secondary are not well measured in 4U 1636-53, as Figure 8 suggests the system is rather well constrained. The lack of eclipses implies that $i \lesssim 76°$. In addition, no dipping or partical eclipses have been observed from 4U 1636-53. The modelling of Frank, King & Lasota (1987) suggests that $i \lesssim 60°$ in such cases. We can combine our limits on the velocity of the neutron star with the radial velocity measurements to place constraints on the component masses. With the known orbital period we have that the neutron star velocity,

$$v_{ns} < \frac{394.5 \ M_1 \ \sin i}{(M_1 + M_2)^{2/3}} \ \text{km s}^{-1}, \tag{2}$$

with v_{ns} set to either our 90 or 99% limit (see §4.3 above). To derive mass constraints from the radial velocity data we required that the inferred location of the radial velocity components (determined from the velocity amplitude and phase of superior conjunction data of Augusteijn et al. 1998, see discussion above) must fit within 90% of the Roche lobe radius of the neutron star (a likely size for the accretion disk). In deriving these locations we assumed that the velocities of the emission line components are dominated by their motions with respect to the center of mass of the binary (see discussion above). Because these constraints are dependent on the accuracy of this assumption we caution that they should be considered as reasonable estimates only.

Our constraints are summarized in Figure 9. We show allowed regions in the component mass plane for a pair of different inclinations (40 and 50°) for our 90 and 99% neutron star velocity limits. Indeed for $v_{ns} \lesssim 38$ km s^{-1} the mass of the secondary must be significantly less than the $0.36 M_\odot$ estimate based on the mass - radius relation for main sequence stars. Further, even if the secondary is $\sim 0.2 M_\odot$ then the neutron star must be quite massive $M_{ns} > 1.8 M_\odot$. The radial velocity constraints suggest that $i \lesssim 40°$ is unlikely for any reasonable masses of the components. This is because the disk cannot be big enough to allow high radial velocities if the inclination is too low. Although this conclusion is dependent on our assumption for deriving the radial velocity constraints, observations of large amplitude oscillations on the rising edge of bursts from this source also indicate that the inclination cannot be too low (see Nath, Strohmayer & Swank 2001). These

arguments suggest a likely range for the inclination of $40° < i < 50°$. With this inclination a likely range of masses for the neutron star and secondary are, in solar units, $1.4 < M_{ns} < 2.0$ and $0.1 < M_{sec} < 0.25$. More precise limits on the radial velocity of either component will allow more precise mass limits to be inferred.

Clearly additional optical photometry and spectroscopy are required for 4U 1636-53. As more burst data become available it should become possible to measure the neutron star velocity. For example, with a factor of ~ 3 increase in the number of bursts with reliable asymptotic periods and with a burst oscillation period measurement uncertainty of 2.2×10^{-4} ms, our simulations suggest that a velocity of 38 km s^{-1} (equal to our current 90% upper limit) can be detected at $\sim 3\sigma$ confidence. Figure 10 shows the results of such a simulation for 54 burst asymptotic period measurements. The individual periods are shown with plus signs. A running average of 6 consecutive periods is shown as the large diamond symbols as well as the best fitting model (dashed line). A constant (zero) velocity model is rejected at $\sim 3\sigma$ in this simulation.

The bursts listed in Table 3 were found in observations totaling ~ 1.2 Msec of exposure. Based on this X-ray burst rate the presently approved RXTE observing time on 4U 1636-53 (1.15 Msec in AO6) can be expected to provide another ~ 28 X-ray bursts, which should roughly double the sample. Since RXTE provides much higher quality X-ray burst profiles than did Hakucho, further attempts to get simultaneous X-ray - optical burst observations are clearly worthwhile but this requires and is dependant on the availability of a large optical telescope.

We thank Holger Pedersen for re-examining and confirming the dates and times of observations of 4U 1636-53 made in 1980. Archive data was obtained from the High Energy Astrophysics Science Archive Research Center Online Service provided by the NASA / Goddard Space Flight Center. We also thank the referees for their informative comments.

REFERENCES

Augusteijn, T., van der Hooft, F., de Jong, J.A., van Kerkwijk, M.H., & van Paradijs, J., 1998, A&A, 332, 561

Bildsten, L. & Cutler, C. 1995, ApJ, 449, 800

Cumming, A. & Bildsten, L. 2000, ApJ, 544, 453

Cumming, A. et al. 2001, ApJ, submitted, (astro-ph/0108009)

Cummings, N. & Strohmayer, T. E. 2001, in preparation

Frank, J., King, A. R. & Lasota, J.-P. 1987, A&A, 178, 137

Giles, A.B., Hill, K.M., & Greenhill, J.G., 1999, MNRAS, 304, 47

Heyl, J. S. 2001, astro-ph/0108450

in't Zand, J. J. M. et al. 2001, A&A, 372, 916

Jernigan, J. G., Apparao, K. M. V., Bradt, H. V., Doxsey, R. E. & McClintock, J. E., 1977, Nature, 270, 321

Lubow, S. H., & Shu, F. H. 1975, ApJ, 198, 383

McClintock, J.E., Canizares, C.R., Bradt, H.V., Doxsey, R.E., Jernigan, J.G., & Hiltner, W.A., 1977, Nature, 270, 320

Miller, M. C. 2000, ApJ, 531, 458

Muno, M. P., Fox, D. W., Morgan, E. H. & Bildsten, L. 2000, ApJ, 542, 1016

Nath, N. R., Strohmayer, T. E. & Swank, J. H. 2001, ApJ, in press, (astro-ph/0102421)

Patterson, J. 1984, ApJS, 54, 443

Pedersen, H. et al., 1982a, ApJ, 263, 325

Pedersen, H., van Paradijs, J., Motch, C., Cominsky, L., Lawrence, A., Lewin, W.H.G., Oda, M., Ohashi, T., & Matsuoka, M., 1982b, ApJ, 263, 340

Smale, A. P. & Mukai, K. 1988, MNRAS, 231, 663

Spitkovsky, A., Levin, Y. & Ushomirsky, G. 2001, ApJ, submitted, (astro-ph/0108074)

Strohmayer, T. E. 2001, Advances Sp. Res. submitted, (astro-ph/0012516)

Strohmayer, T. E. & Lee, U. 1996, ApJ, 467, 773

Strohmayer, T.E., Zhang, W., Swank, J.H., Smale, A.P., Titarchuk, L., Day, C., & Lee, U., 1996, ApJ, 469, L9

Strohmayer, T.E., Zhang, W., & Swank, J.H., 1997, ApJ, 487, L77

Strohmayer, T. E., Jahoda, K., Giles, A. B. & Lee, U. 1997, ApJ, 486, 355

Strohmayer, T. E., Zhang, W., Swank, J. H., White, N. E. & Lapidus, I. 1998a, ApJ, 498, L135

Strohmayer, T.E., Zhang, W., Swank, J.H., & Lapidus, I., 1998b, ApJ, 503, L147

Strohmayer, T.E., Swank, J.H., & Zhang, W., 1998, Nuclear Phys B (Proc. Suppl.), 69/1-3, 129-134

Strohmayer, T.E., & Markwardt, C.B., 1999, ApJ, 516, L81

Strohmayer, T. E. 1999, ApJ, 523, L51

van Paradijs J., 1983, in Accretion-driven Stellar X-ray Sources, ed. W.H.G. Lewin & E.P.T. van den Heuval, Cambridge University Press, Cambridge, 191

van Paradijs J., & McClintock J.E., 1995, in X-ray Binaries, ed. W.H.G. Lewin, J. van Paradijs, & E.P.T. van den Heuval, Cambridge University Press, Cambridge, 58

van Paradijs, J., van der Klis, M., van Amerongen, S., Pedersen, H., Smale, A.P., Mukai, K., Schoembs, R., Haefner, R., Pfeiffer, M., & Lewin, W.H.G., 1990, A&A, 234, 181

Figure Captions

Fig. 1.— The V band light curves for 4U 1636-53 on 1998 March 25 & 27 and 1998 April 3. The solid traces through the data points mark our best fit sine curves. The dotted curves show the ephemeris predictions of Augusteijn et al. (1998) for the same three nights with an arbitrary offset and amplitude. The number in each panel refers to the HJD starting at zero hours within each light curve. Note that the horizontal extent of the symbols is not meant to indicate an error bar.

Fig. 2.— The V band light curves for 4U 1636-53 on 1999 June 9 and 2001 May 7 & 8. The solid traces through the data points mark our best fit sine curves. The dotted curves show the ephemeris predictions of Augusteijn et al. (1998) for the same three nights with an arbitrary offset and amplitude. The number in each panel refers to the HJD starting at zero hours within each light curve. Note that the horizontal extent of the symbols is not meant to indicate an error bar.

Fig. 3.— The observed minus calculated (O-C) times of maximum optical light for 4U 1636-53 plotted against time. The points after HJD 2450000 are from Table 2 and the earlier data are taken from Table 2 in Augusteijn et al. (1998). The ephemeris parameters have been adjusted to place the best linear fit through the data points to lie along the zero phase axis. The ephemeris for the time of maximum light is then HJD = 2446667.3179(33) $\pm$ [N $\times$ 0.15804693(16)]. A higher order polynomial fit to the widely scattered data points is not warranted. Note that the horizontal extent of the symbols is not meant to indicate an error bar.

Fig. 4.— Dynamic Z_1^2 spectrum in the hard X-ray band (7 - 20 keV) for burst number 20 in Table 3 (top). The horizontal dashed line marks the asymptotic period inferred for this burst. The burst lightcurve is overlaid (right axis). The gaps in the lightcurve are due to telemetry limitations for this data mode. Also shown is the Z_1^2 spectrum in the tail of the burst from which the asymptotic period was measured (bottom). In this case the vertical dashed line marks the asymptotic period.

Fig. 5.— Histogram of simulated period measurements and best fitting gaussian distribution. See the text (§4.1) for a discussion of the simulations. The fixed period used for the simulation was 1.7196 ms. The width of the gaussian is 2.2×10^{-4} ms and represents the characteristic uncertainty in our asymptotic period measurements.

Fig. 6.— Histogram of measured asymptotic burst oscillation periods for 4U 1636-53. The periods are corrected to the solar system barycenter. Note the cluster of 18 periods centered near 1.7192 ms. A gaussian distribution centered at 1.71929 ms, of width $\sigma = 2.3 \times 10^{-4}$ ms fits these data well and is shown by the thick solid curve. Note the presence of outliers towards longer period, but none shortward of the gaussian.

Fig. 7.— Plot of asymptotic period versus orbital phase for the subset of 18 bursts which have a tightly clustered period distribution. Phase zero corresponds to maximum optical light. The solid curve is the best fitting doppler model with $v_{ns} \sin i = 16.5$ km s^{-1} and the phase, ϕ_{dyn}, of maximum period redshift fixed at 0.25. This fit, however, is not statistically significant compared

to one with $v_{ns} \sin i = 0$ (see §4.3). The dashed curves show the models with $v_{ns} \sin i = 38$ and 50 km s^{-1}, which are equal to our 90% and 99% confidence upper limits. The dotted curve shows the best fitting model with ϕ_{dyn} as an additional free parameter. This fit has $v_{ns} \sin i = 35.4$ km s^{-1}.

Fig. 8.— Diagram of the Roche geometry for 4U 1636-53. The figure was drawn assuming neutron star and secondary masses of $1.6 M_{\odot}$ and $0.36 M_{\odot}$, respectively. The system rotates clockwise in this depiction. The numbers circling the components correspond to orbital phases under the assumption that phase zero corresponds to superior conjunction of the secondary (V801 Arae). We note that this does not necessarily correspond to the phase of photometric maximum. The center of mass (CM) is denoted by a square symbol. The dashed circle around the neutron star marks the likely extent of an accretion disk under the assumption that it fills 90% of the neutron star Roche lobe. The triangles and shaded region mark the inferred locations of the radial velocity components measured by Augusteijn et al. (1998).

Fig. 9.— Constraints on the component masses in 4U 1636-53 derived from our upper limit on $v_{ns} \sin i$ and the radial velocity data of Augusteijn et al. (1998). The regions with horizontal hatching are excluded by the neutron star velocity limit, while the vertical hatched regions are excluded by the radial velocity data. We show constraints for $i = 40°$ and $v_{ns} \sin i < 38$ km s^{-1} (a), $i = 40°$ and $v_{ns} \sin i < 50$ km s^{-1} (b), $i = 50°$ and $v_{ns} \sin i < 38$ km s^{-1} (c), $i = 50°$ and $v_{ns} \sin i < 50$ km s^{-1} (d). The thick lines denote $M_{ns} = 1.4 M_{\odot}$ and $M_{sec} = 0.36 M_{\odot}$, respectively. See §5.1 for a discussion of how the constraints were derived.

Fig. 10.— Period versus orbital phase simulation using 54 simulated asymptotic periods (plus sign symbols) sampled with the same statistical uncertainty as we estimated for our real measurements . We used a velocity of 38 km s^{-1}, equal to our 90% confidence limit. Averages of 6 consecutive simulated measurements are shown as the large diamond symbols. We also show the best fitting orbital doppler model (dashed curve). The neutron star velocity is detected at 3σ confidence in this simulation. This suggests that a factor of ~ 3 increase in the number of observed asymptotic periods should enable a detection of the neutron star velocity.

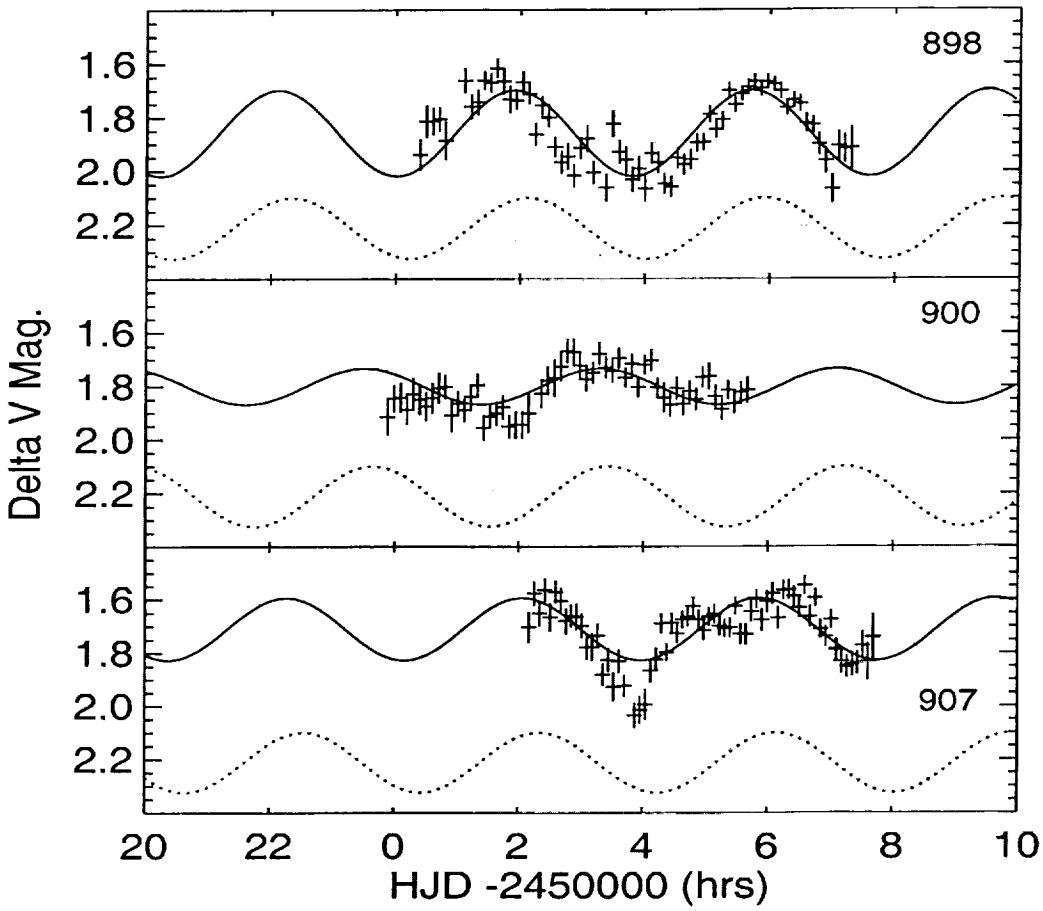

Figure 1: The V band light curves for 4U 1636-53 on 1998 March 25 & 27 and 1998 April 3. The solid sine curve marks our new ephemeris with a period of 3.70312064 hours. The dotted curve shows the ephemeris prediction of Augusteijn et al. (1998) for the same three nights with an arbitrary offset and amplitude. The number in each panel refers to the HJD starting at zero hours within each light curve. Note that the horizontal extent of the symbols is not meant to indicate an error bar.

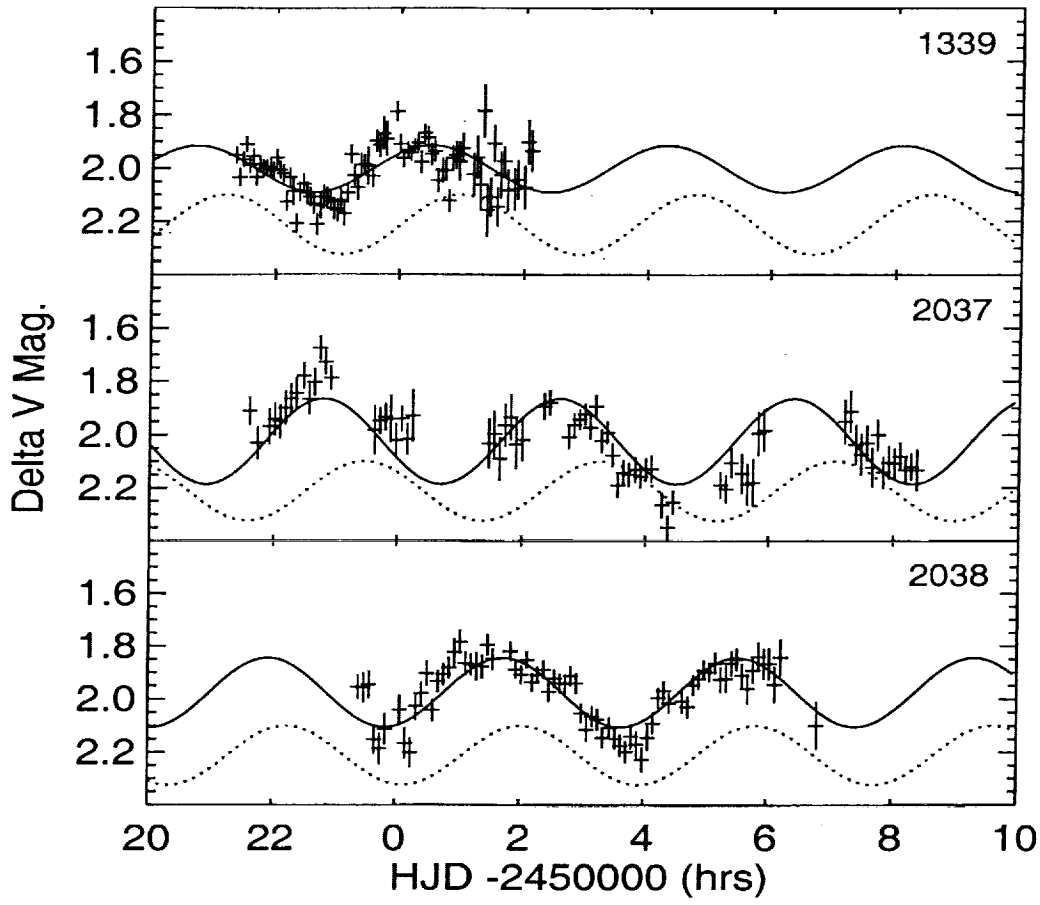

Figure 2: The V band light curves for 4U 1636-53 on 1999 June 9 and 2001 May 7 & 8. The solid sine curve marks our new ephemeris and the first optical maximum on 7 May occurs at HJD = 2452036.954706 The dotted curve shows the ephemeris prediction of Augusteijn et al. (1998) for the same three nights with an arbitrary offset and amplitude. The number in each panel refers to the HJD starting at zero hours within each light curve. Note that the horizontal extent of the symbols is not meant to indicate an error bar.

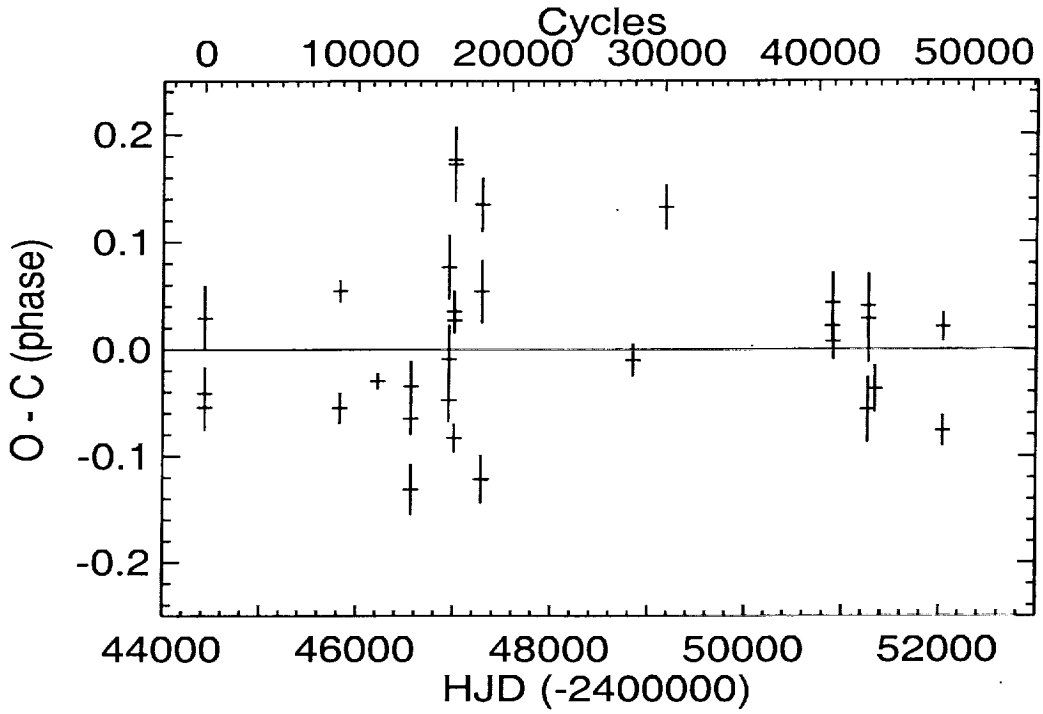

Figure 3: The observed minus calculated (O-C) times of maximum optical light for 4U 1636-53 plotted against time. The points after HJD 2450000 are from Table 2 and the earlier data are taken from Table 2 in Augusteijn et al. (1998). The ephemeris parameters have been adjusted to place the best linear fit through the data points to lie along the zero phase axis. The ephemeris for the time of maximum light is then HJD = 2446667.3179(33) $\pm$ [N $\times$ 0.15804693(16)]. A higher order polynomial fit to the widely scattered data points is not warranted. Note that the horizontal extent of the symbols is not meant to indicate an error bar.

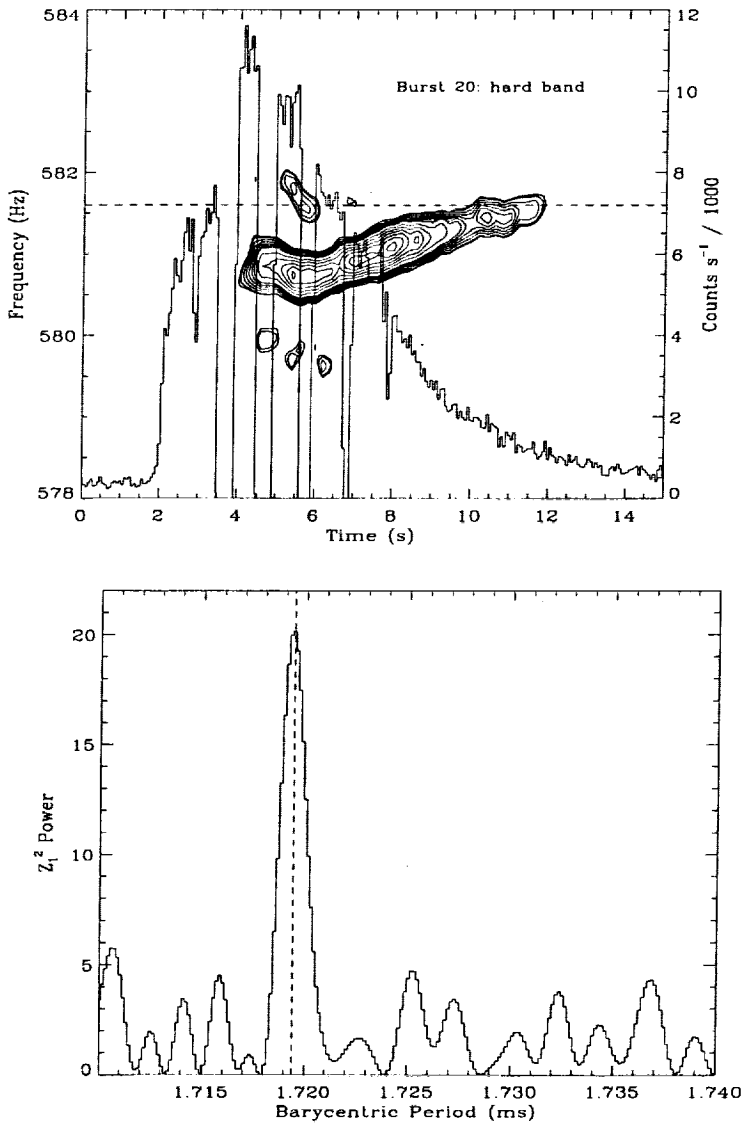

Figure 4: Dynamic Z_1^2 spectrum in the hard X-ray band (7 - 20 keV) for burst number 20 in Table 3 (top). The horizontal dashed line marks the asymptotic period inferred for this burst. The burst lightcurve is overlaid (right axis). The gaps in the lightcurve are due to telemetry limitations for this data mode. Also shown is the Z_1^2 spectrum in the tail of the burst from which the asymptotic period was measured (bottom). In this case the vertical dashed line marks the asymptotic period.

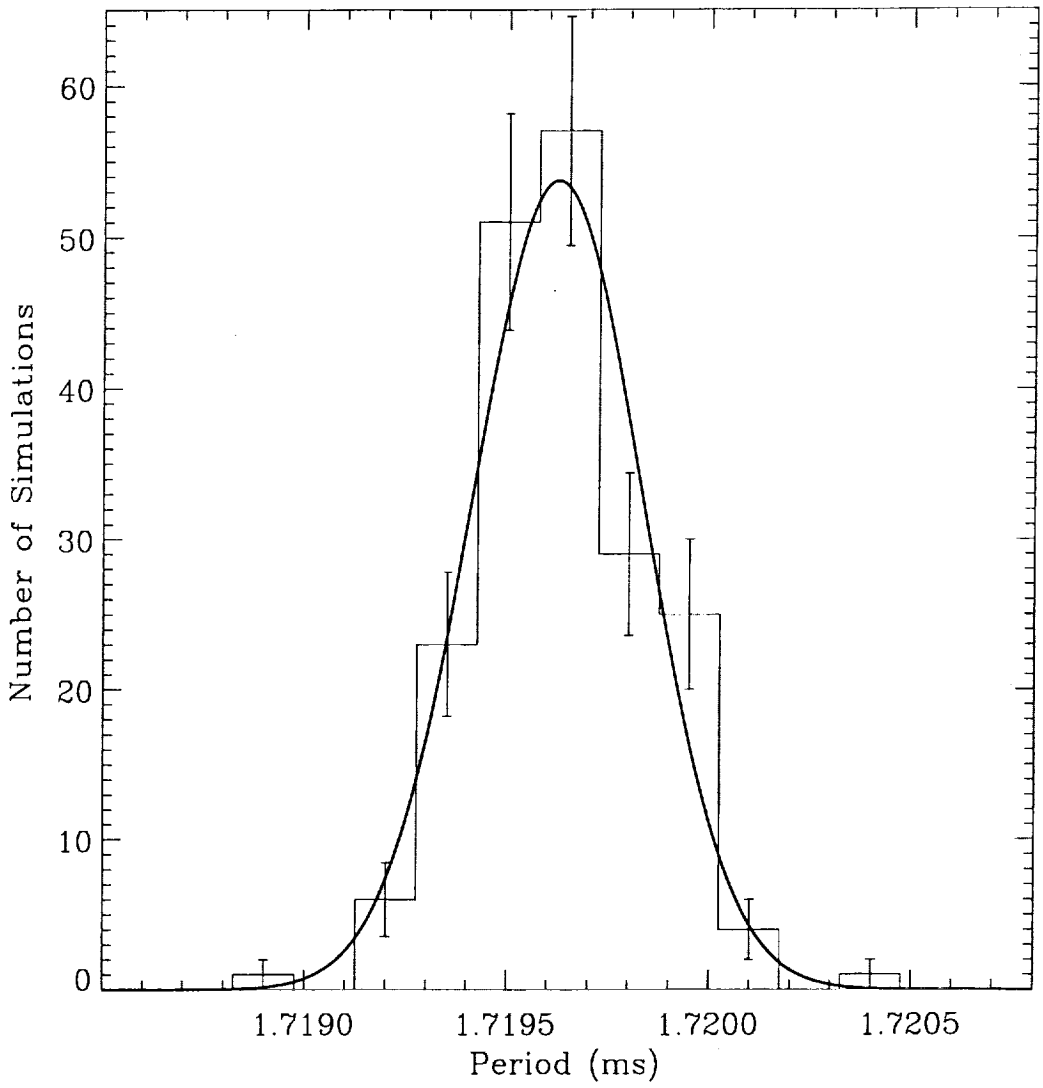

Figure 5: Histogram of simulated period measurements and best fitting gaussian distribution. See the text (§4.1) for a discussion of the simulations. The fixed period used for the simulation was 1.7196 ms. The width of the gaussian is 2.2×10^{-4} ms and represents the characteristic uncertainty in our asymptotic period measurements.

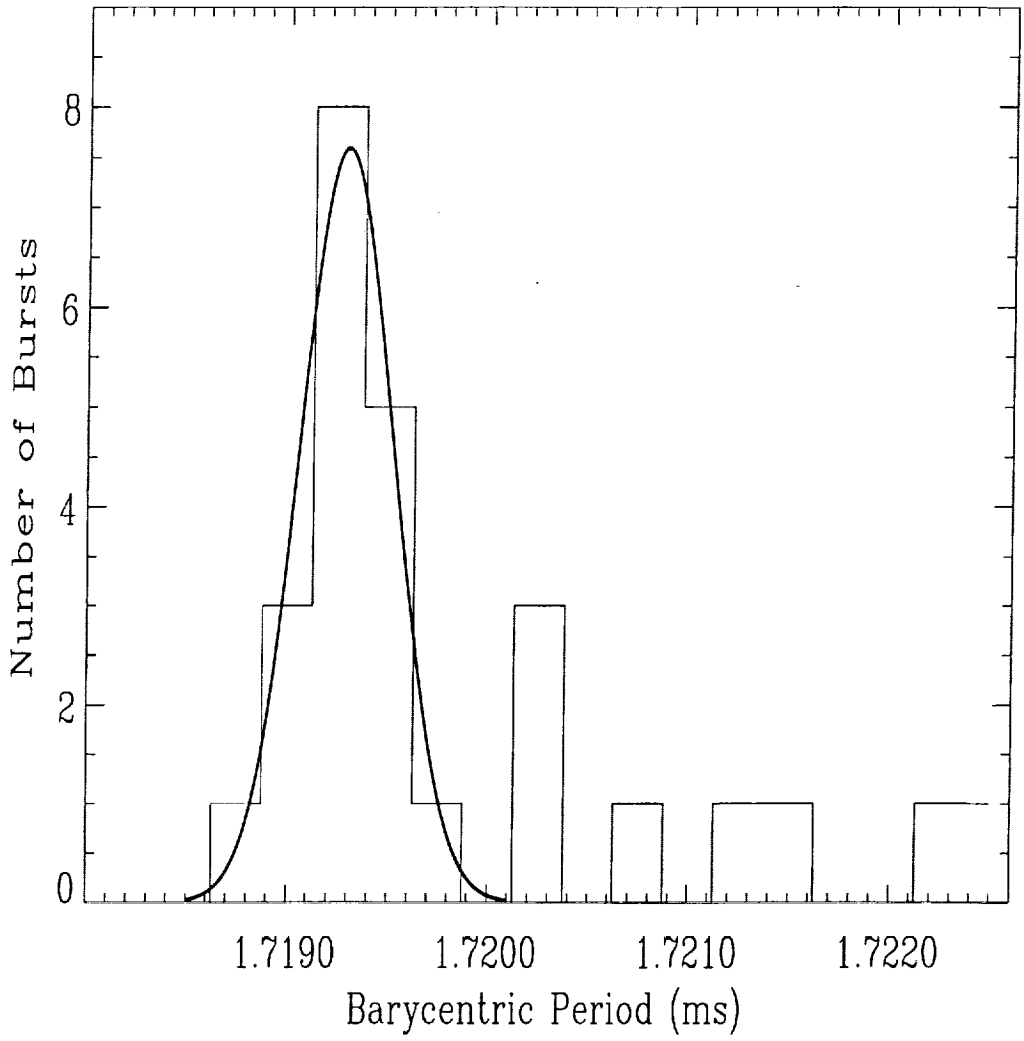

Figure 6: Histogram of measured asymptotic burst oscillation periods for 4U 1636-53. The periods are corrected to the solar system barycenter. Note the cluster of 18 periods centered near 1.7192 ms. A gaussian distribution centered at 1.71929 ms, of width $\sigma = 2.3 \times 10^{-4}$ ms fits these data well and is shown by the thick solid curve. Note the presence of outliers towards longer period, but none shortward of the gaussian.

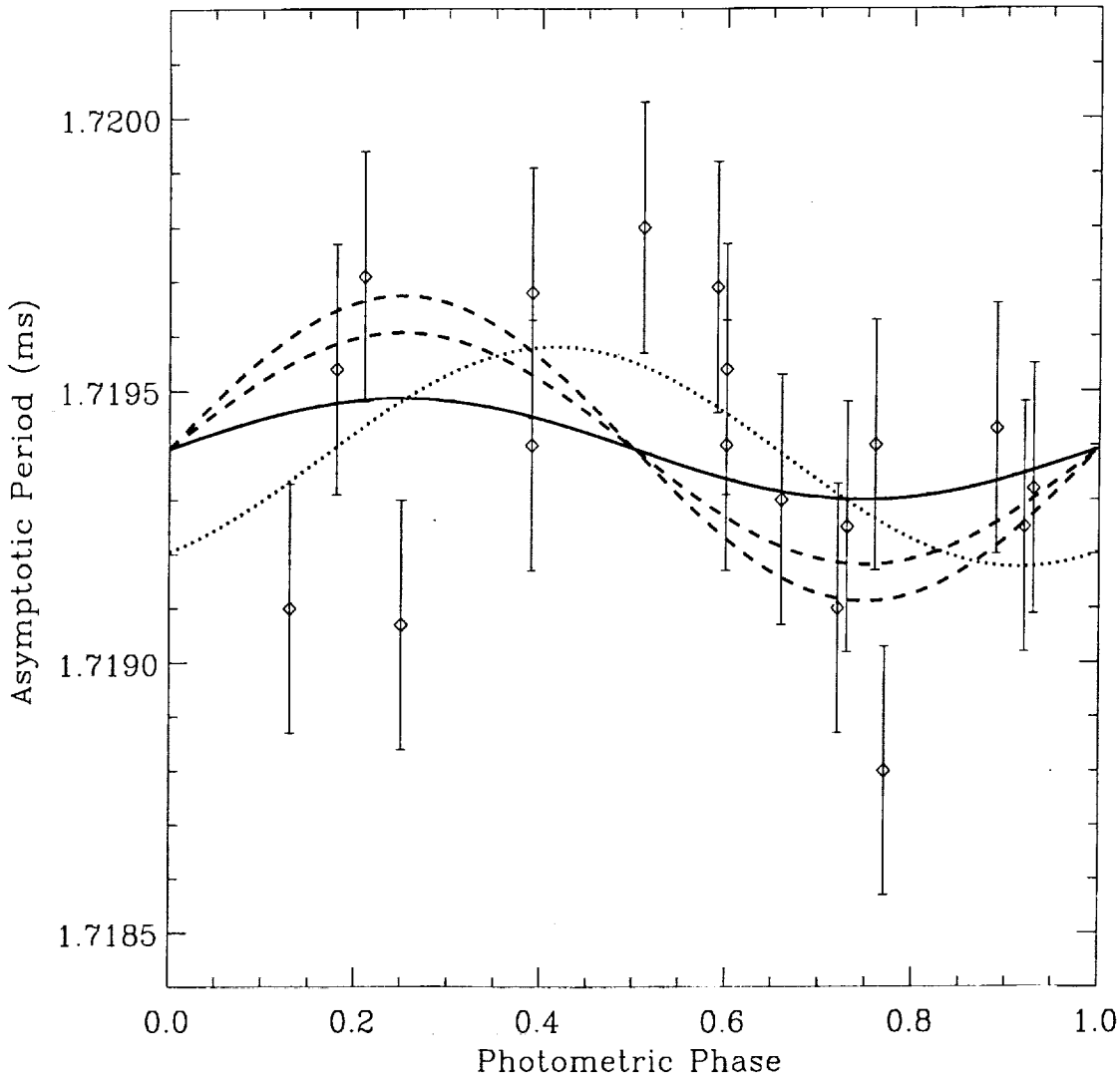

Figure 7: Plot of asymptotic period versus orbital phase for the subset of 18 bursts which have a tightly clustered period distribution. Phase zero corresponds to maximum optical light. The solid curve is the best fitting doppler model with $v_{ns} \sin i = 16.5$ km s^{-1} and the phase, ϕ_{dyn}, of maximum period redshift fixed at 0.25. This fit, however, is not statistically significant compared to one with $v_{ns} \sin i = 0$ (see §4.3). The dashed curves show the models with $v_{ns} \sin i = 38$ and 50 km s^{-1}, which are equal to our 90% and 99% confidence upper limits. The dotted curve shows the best fitting model with ϕ_{dyn} as an additional free parameter. This fit has $v_{ns} \sin i = 35.4$ km s^{-1}.

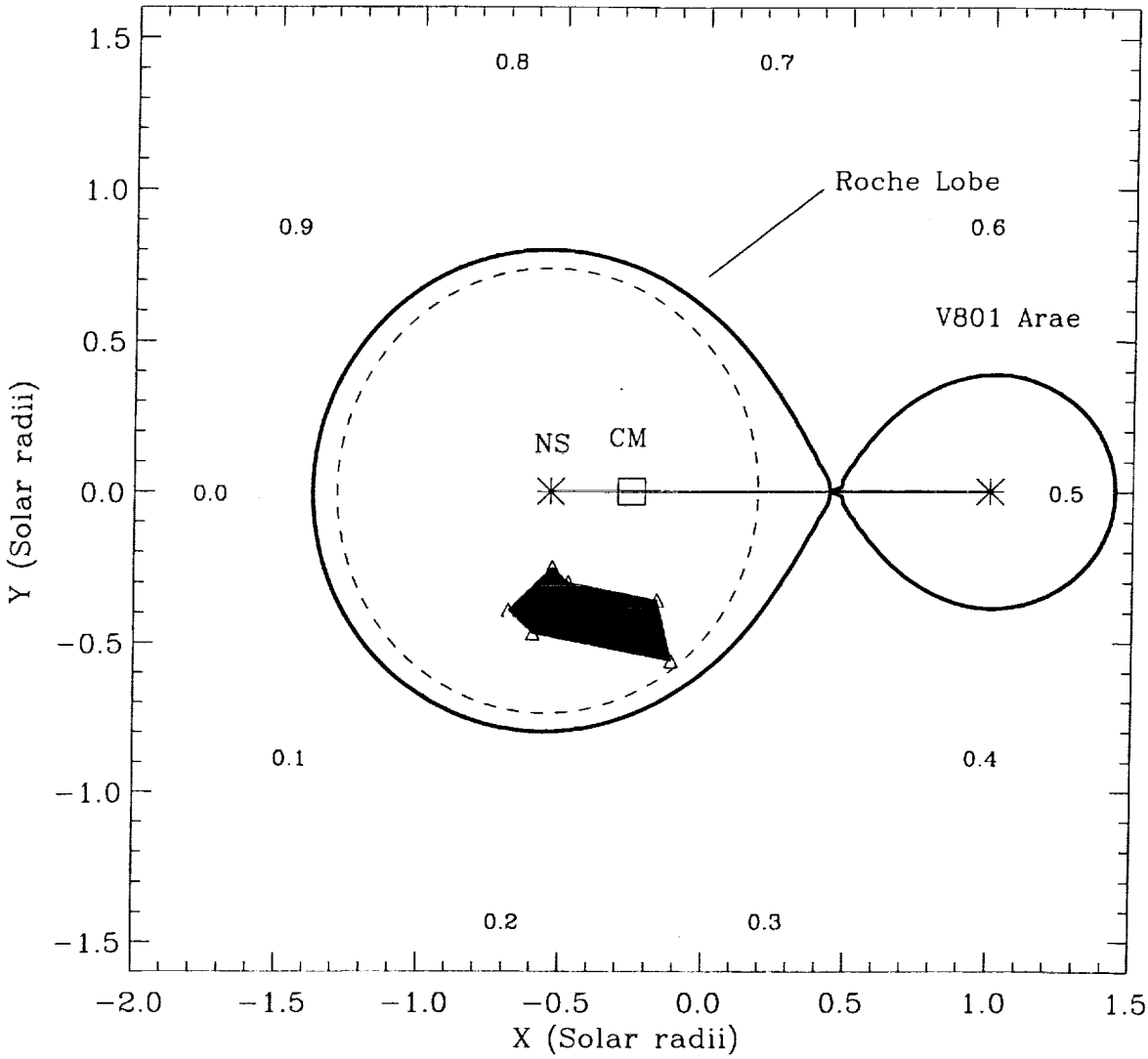

Figure 8: Diagram of the Roche geometry for 4U 1636-53. The figure was drawn assuming neutron star and secondary masses of $1.6M_{\odot}$ and $0.36M_{\odot}$, respectively. The system rotates clockwise in this depiction. The numbers circling the components correspond to orbital phases under the assumption that phase zero corresponds to superior conjunction of the secondary (V801 Arae). We note that this does not necessarily correspond to the phase of photometric maximum. The center of mass (CM) is denoted by a square symbol. The dashed circle around the neutron star marks the likely extent of an accretion disk under the assumption that it fills 90% of the neutron star Roche lobe. The triangles and shaded region mark the inferred locations of the radial velocity components measured by Augusteijn et al. (1998).

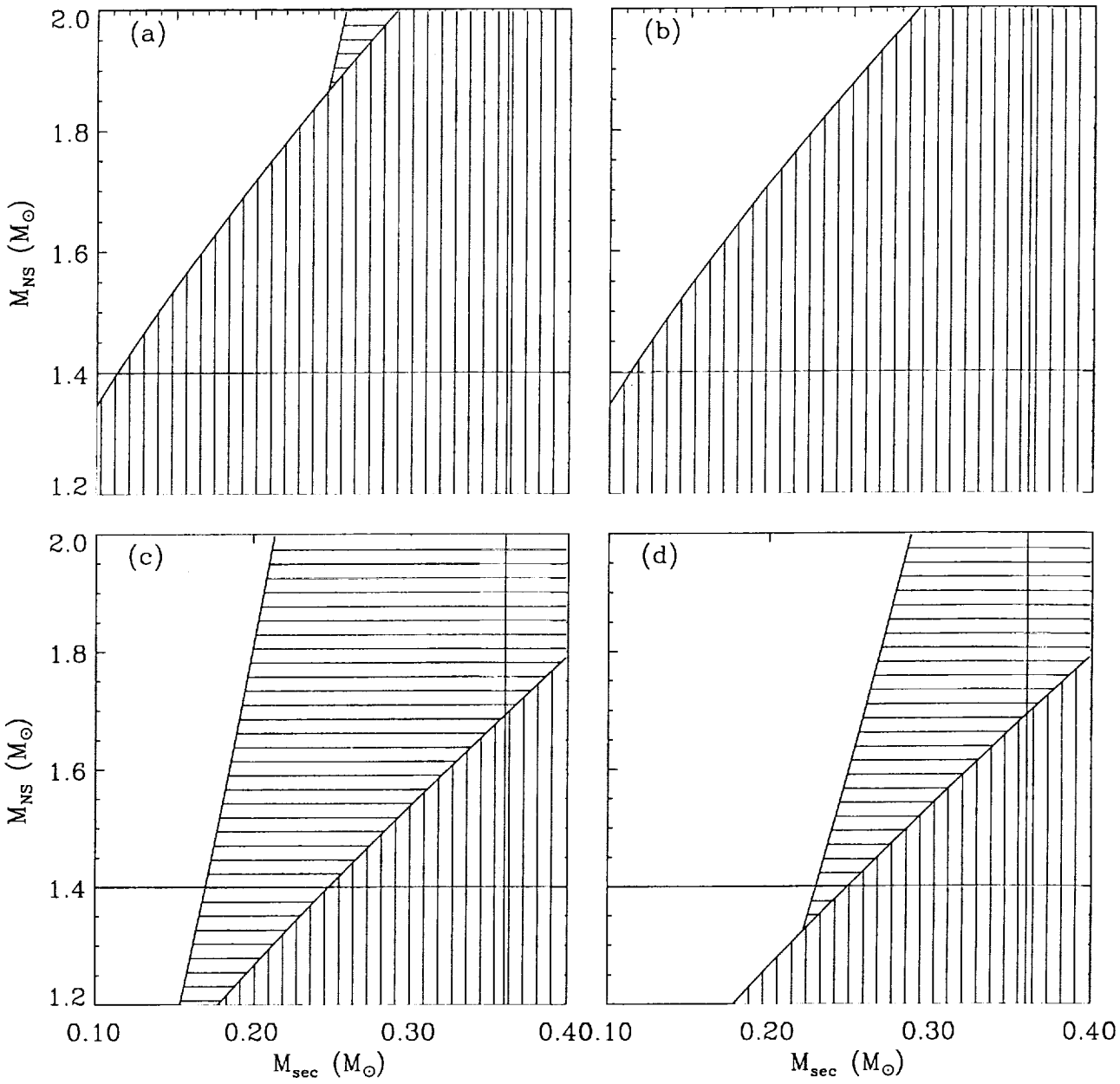

Figure 9: Constraints on the component masses in 4U 1636-53 derived from our upper limit on $v_{ns} \sin i$ and the radial velocity data of Augusteijn et al. (1998). The regions with horizontal hatching are excluded by the neutron star velocity limit, while the vertical hatched regions are excluded by the radial velocity data. We show constraints for $i = 40°$ and $v_{ns} \sin i < 38$ km s^{-1} (a), $i = 40°$ and $v_{ns} \sin i < 50$ km s^{-1} (b), $i = 50°$ and $v_{ns} \sin i < 38$ km s^{-1} (c), $i = 50°$ and $v_{ns} \sin i < 50$ km s^{-1} (d). The thick lines denote $M_{ns} = 1.4 M_\odot$ and $M_{sec} = 0.36 M_\odot$, respectively. See §5.1 for a discussion of how the constraints were derived.

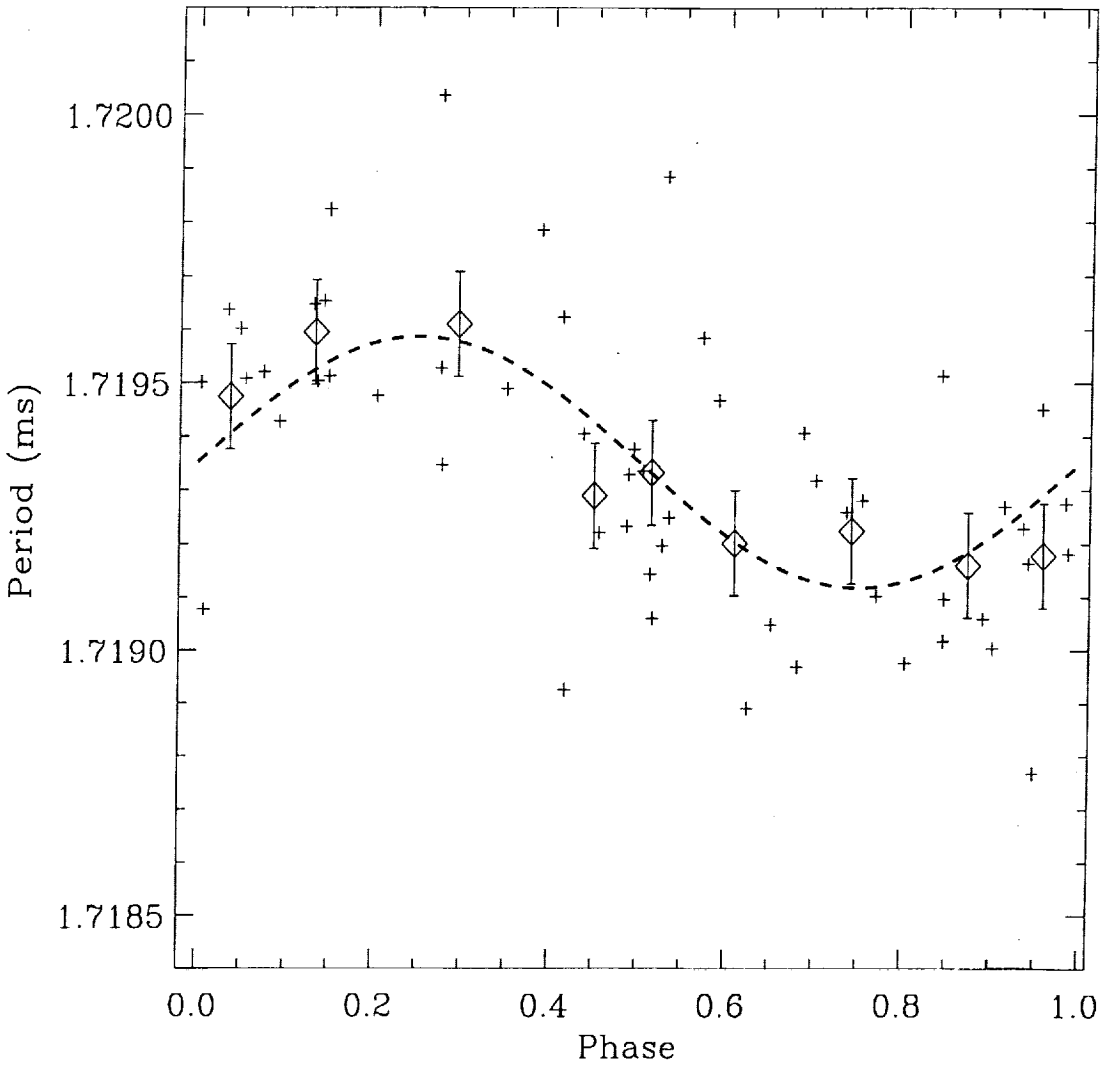

Figure 10: Period versus orbital phase simulation using 54 simulated asymptotic periods (plus sign symbols) sampled with the same statistical uncertainty as we estimated for our real measurements . We used a velocity of 38 km s^{-1}, equal to our 90% confidence limit. Averages of 6 consecutive simulated measurements are shown as the large diamond symbols. We also show the best fitting orbital doppler model (dashed curve). The neutron star velocity is detected at 3σ confidence in this simulation. This suggests that a factor of ~ 3 increase in the number of observed asymptotic periods should enable a detection of the neutron star velocity.

Table 1: Optical observations of 4U 1636-53

Date	HJD Start -2450000	HJD End -2450000	Filter	Int. (s)	No. Exp.
3/25/98	0898.01619	0898.30426	*V* & *I*	180	65
3/27/98	0899.99518	0900.23595	*V* & *I*	180	56
4/ 3/98	0907.09065	0907.32071	*V*	300	65
3/26/99	1264.02547	1264.30913	*V*	300	32
3/28/99	1266.15552	1266.26166	*V*	300	10
3/31/99	1269.15566	1269.29098	*V*	300	16
4/ 2/99	1271.08660	1271.32108	*V*	300	33
4/ 4/99	1273.25977	1273.31819	*V*	300	8
6/ 9/99	1338.88939	1339.14694	*V*	180	81
6/10/99	1340.18839	1340.27722	*V*	180	12
5/ 7/01	2036.89853	2037.34667	*V*	300	72
5/ 8/01	2037.97337	2038.28175	*V*	300	74

Table 2: Times of maximun optical light for 4U 1636-53

Date	Cycle No.	HJD -2450000	Error (day)
3/25/98	40915	0898.0796	0.0022
3/27/98	40928	0900.1376	0.0045
4/ 3/98	40972	0907.0860	0.0027
3/26/99	43231	1264.1039	0.0049
3/28/99	43244	1266.1738	0.0048
4/ 2/99	43275	1271.0714	0.0065
6/ 9/99	43705	1339.0212	0.0035
5/ 7/ 1	48122	2037.1083	0.0023
5/ 8/ 1	48128	2038.0720	0.0021

Table 3: X-ray bursts detected from 4U 1636-53 by RXTE

Burst No.	RXTE Obs. ID.	Date	HJD -2450000	Period (ms) ± 0.00040	Binary phase ± 0.04
1	10088-01-07-02	12/28/96	0446.439466	1.71940	0.39
2	10088-01-07-02	12/28/96	0446.491308	1.71910	0.72
3	10088-01-08-01	12/29/96	0447.472404	1.71925	0.92
4	10088-01-08-030	12/31/96	0449.229474	-	0.04
5	10088-01-09-01	2/23/97	0502.913912	1.72028	0.72
6	30053-02-02-02	8/19/98	1044.991053	1.72083	0.57
7	30053-02-01-02	8/20/98	1045.654542	1.72161	0.76
8	30053-02-02-00	8/20/98	1045.719849	1.71954	0.18
9	40028-01-02-00	2/27/99	1236.865609	1.71954	0.60
10	40028-01-04-00	4/29/99	1297.575867	1.71925	0.73
11	40028-01-06-00	6/10/99	1339.751875	1.72240	0.59
12	40028-01-08-00	6/18/99	1348.493173	1.71943	0.89
13	40030-03-04-00	6/19/99	1349.234723	1.72260	0.59
14	40031-01-01-06	6/21/99	1351.300601	1.71930	0.66
15	40028-01-10-00	9/25/99	1447.360320	-	0.45
16	40028-01-13-00	1/22/00	1565.570419	-	0.39
17	40028-01-13-00	1/22/00	1565.703136	1.72043	0.23
18	40028-01-14-01	1/30/00	1573.506255	-	0.60
19	40028-01-15-00	6/15/00	1710.717286	1.72147	0.77
20	40028-01-18-000	8/ 9/00	1765.557103	1.71940	0.76
21	40028-01-18-00	8/ 9/00	1765.875286	1.71880	0.77
22	40028-01-19-00	8/12/00	1769.482989	1.71940	0.60

Table 3 (cont.): X-ray bursts detected from 4U 1636-53 by RXTE

Burst No.	RXTE Obs. ID.	Date	HJD -2450000	Period (ms) ± 0.00040	Binary phase ± 0.04
23	40028-01-20-00	10/03/00	1821.479052	1.71969	0.59
24	50030-02-01-00	11/05/00	1853.677829	1.72043	0.32
25	50030-02-02-00	11/12/00	1861.247296	1.71971	0.21
26	50030-02-04-00	1/28/01	1937.613090	1.71968	0.39
27	50030-02-05-01	2/01/01	1942.372888	1.71980	0.51
28	50030-02-05-00	2/02/01	1942.597558	1.71932	0.93
29	50030-02-09-000	4/05/01	2005.215668	1.71910	0.13
30	50030-02-10-00	4/30/01	2029.732151	1.71907	0.25